ELSEVIER

Contents lists available at ScienceDirect

Analytical Biochemistry

journal homepage: www.elsevier.com/locate/yabio



Development of sterile platform for quantification of extracellular analytes via single walled carbon nanotubes

Ivon Acosta-Ramirez ^a, Carley Conover ^a, Jacob Larsen ^b, Portia N.A. Plange ^a, Ufuk Kilic ^c, Becca Muller ^a, Nicole M. Iverson ^{a,*}

- Department of Biological Systems Engineering, College of Agricultural Sciences and Natural Resources, University of Nebraska-Lincoln, 4240 Fair St, Lincoln NE, 68504, United States
- b Department of Chemistry, College of Arts and Sciences, University of Nebraska-Lincoln, 639 N 12th Street, Lincoln NE, 68508, United States
- c Department of Electrical and Computer Engineering, University of Nebraska-Lincoln, 900 N 16th St, Lincoln NE, 68508, United States

ARTICLEINFO

Keywords:

Single walled carbon nanotubes Immobilization method Extracellular analytes Biosensors Nanoarrays Biocompatibility

ABSTRACT

Progress has been made studying cell-cell signaling communication processes. However, due to limitations of current sensors on time and spatial resolution, the role of many extracellular analytes is still unknown. A single walled carbon nanotube (SWNT) platform was previously developed based on the avidin-biotin immobilization of SWNT to a glass substrate. The SWNT platform provides real time feedback about analyte concentration and has a high concentration of evenly distributed sensors, both of which are essential for the study of extracellular analytes. Unfortunately, this initial SWNT platform is synthesized through unsterile conditions and cannot be sterilized post-production due to the delicate nature of the sensors, making it unsuitable for in vitro work. Herein the multiple-step process for SWNT immobilization is modified and the platform's biocompatibility is assessed in terms of sterility, cytotoxicity, cell proliferation, and cell morphology through comparison with non-sensors controls. The results demonstrate the SWNT platform's sterility and lack of toxicity over 72 h. The proliferation rate and morphology profiles for cells growing on the SWNT platform are similar to those grown on tissue culture substrates. This novel nano-sensor platform preserves cell health and cell functionality over time, offering opportunities to study extracellular analytes gradients in cellular communication.

1. Introduction

Cellular communication, the transmitting, receiving, and processing of signals, is vital for healthy cell and tissue function [1,2]. It is known that cells communicate through the release of specific concentrations of various analytes [1,2], but the concentration and temporal profiles of many of the analytes involved in cellular communication are unknown, possibly due to the lack of temporal and nanoscale spatial sensors for the highly bioactive molecules that are frequently used in cellular communication. Single walled carbon nanotubes (SWNT) are both small in size and can act as real-time sensors [3], making them ideal candidates for the quantification of extracellular analytes involved in cellular communication.

SWNT are pure carbon structures with unique electronic and optical properties directly related to the orientation of the SWNT's carbon bonds, known as chirality [4]. When fluorescent SWNT are excited by

visible light (400-800 nm) they fluoresce in the near infrared (nIR) region (900-1500 nm) [3,5]. Carbon nanotubes are hydrophobic, but can be functionalized with different wrappings, including polymers and DNA oligomers, to create a hydrophilic compound suitable for use in biological settings [6]. Moreover, by wrapping the SWNT it can be made to react to specific analytes, creating a sensor that changes intensity and/or wavelength of the fluorescence signal when exposed to the analyte [7]. Once the analyte of interest is removed from the SWNT, the fluorescent intensity/wavelength returns to its pre-exposure level. The fluorescence of the SWNT sensor is not permanently altered by interacting with the analyte of interest, so it can be used for repeated sensing events [7]. The library of analytes detected by SWNT continues to expand, some of these analytes are metal ions [8], reactive oxygen species (ROS) [9], reactive nitrogen species (RNS) [10], neurotransmitters [11], lipids [12], proteins [13], and other biomolecules crucial in cell signaling processes [14].

E-mail addresses: iacostaramirez2@huskers.unl.edu (I. Acosta-Ramirez), cconover4@huskers.unl.edu (C. Conover), jlarsen22@huskers.unl.edu (J. Larsen), pplange2@huskers.unl.edu (P.N.A. Plange), ufukkilic@unl.edu (U. Kilic), iverson@unl.edu (N.M. Iverson).

^{*} Corresponding author.

In addition to the functional properties, the structural characteristics of SWNT contribute to their unique capabilities. SWNT's small size, varying from 0.6 to 1.3 nm in diameter and lengths up to 550 mm [15, 16], provides uniform spatial distribution information within micrometer distances and allows gradient profiles to be determined [12,17]. However, SWNT is easily internalized by cells due to its small size [17]. To study extracellular analytes, it is necessary to arrest or immobilize the carbon nanotube onto a substrate without affecting their sensing functionality.

Multiple ways of immobilizing nanoparticles to substrates are based on covalent interactions, however, covalent binding of the SWNT leads to a change in the electron dynamics, impacting the fluorescent functionality of the sensors [6]. To avoid covalent binding, non-covalent interactions, primarily involving electrostatic forces, are frequently used when working with SWNT. Specifically, the electrostatic interac- tion between the positively charged 3-aminopropyl triethoxysilane (APTES) and the negatively charged DNA backbone of the SWNT wrapping, has been used in multiple studies [11,18]. Unfortunately, electrostatic interactions provide low spatial distribution, decreasing the sensor's capability to analyze spatial changes in extracellular analytes [11,19]. Carbon nanotubes can also be immobilized within hydrogels to avoid covalent binding, but this method decreases either the real-time sensing and/or spatial capabilities [20-23]. We recently used the avidin-biotin non-covalent interaction to immobilize SWNT on glass substrates by wrapping the SWNT with biotinylated DNA and attaching avidin to the glass slides [24]. The SWNT-glass platform has a high concentration and even distribution of SWNT, which has the potential to

provide a spatial and temporal understanding of the extracellular analytes' role in cell-cell communication [24]. However, the previously developed platform is synthesized through various non-sterile steps. Since microbial contamination can alter cell population dynamics and extracellular analyte concentrations, the non-sterile method for making the platforms is unsuitable for use with cells.

Various methods of sterilizing bio-scaffolds exists, including the use of organic solvent immersion [25], UV exposure [26,27], high temperature, and high pressure treatments [28]. However, for our specific application of sterilizing the SWNT platform, these methods will not work since they can damage the biomolecule-based SWNT wrapping, altering the sensor properties [29,30]. Therefore, we modified the SWNT immobilization process to create a sterile and biocompatible sensor platform for in vitro experimentation, Fig. 1a.

The biocompatibility of the platform was assessed based on cytotoxicity, proliferation, and morphology changes in cells growing on the SWNT platform. This new SWNT platform (SWNT) was compared with glass slides before the immobilization process (GLASS) and tissue culture treated plates (PLATE), since they can serve as a control to see the impact of the SWNT on the cells (GLASS) and as the standard cell growth platform (PLATE); Fig. 1b shows an overview of these three conditions. The present work demonstrates the capability of the new SWNT plat-form to provide a biocompatible system for spatial and temporal detection of extracellular analytes.

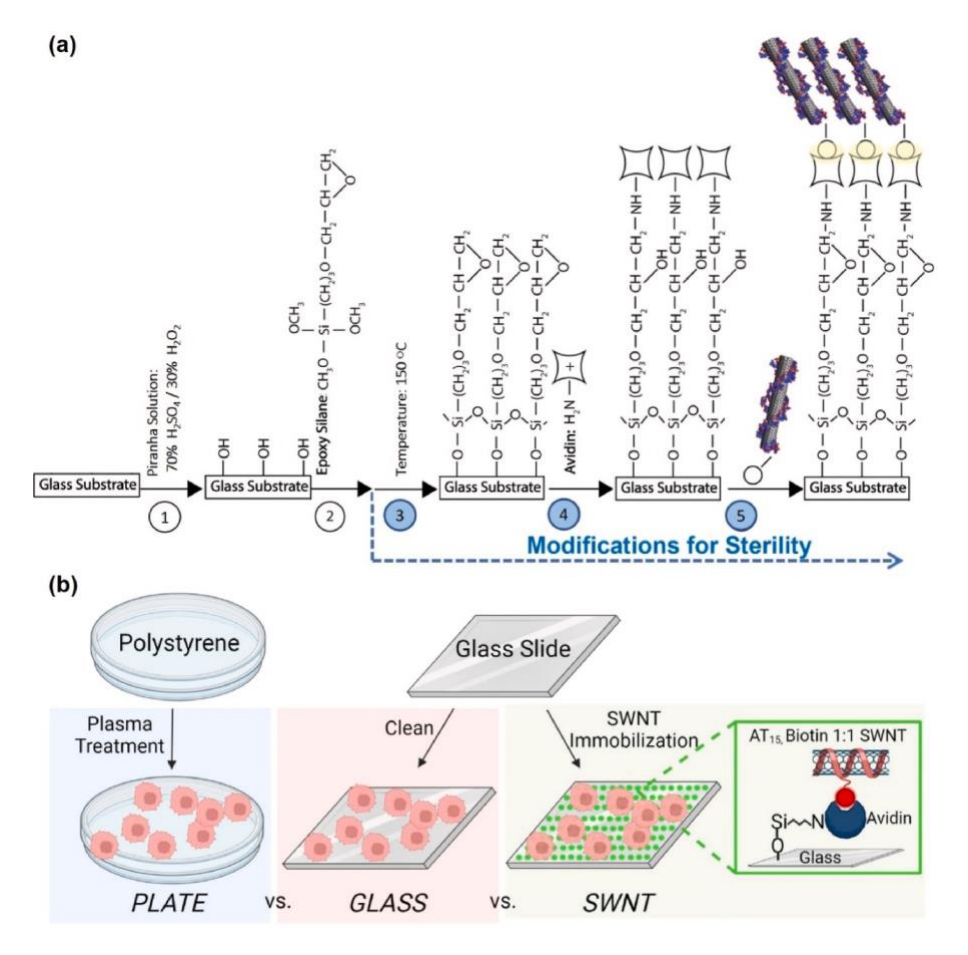


Fig. 1. (a) Illustration of the multiple-step process to immobilize SWNT on a glass slide with modifications from the original non-sterile technique introduced from step 3 to ensure sterility. (b) Schematic of the assessment of the modified SWNT immobilization method as a substrate for in vitro studies. Cellular functionality on *SWNT* was compared with two other substrates: *GLASS* (prior to SWNT immobilization) and *PLATE* (which is known to promote cell growth). Created with Biorender

2. Material and methods

SWNT functionalization: SWNT were dispersed with DNA oligos according to methods previously described [10,31]. Briefly, CoMoCAT 6,5 SWNT (Sigma) were suspended with single stranded DNA in a 2:1 mass ratio in nanopure water. The DNA oligos used were a 1:1 volumetric ratio of (AT)₁₅ and 5'-biotinylated (AT)₁₅ oligos (Integrated DNA Technologies). The suspension was bath-sonicated for 10 min, followed by ultrasonication for 40 min using a 3 mm probe-tip sonicator to unbundle and disperse individual nanotubes and promote DNA functionalization. Subsequently, the solution was centrifuged for 180 min at 16, 100 RCF to remove any unwrapped SWNTs in the supernatant.

Fabrication of biocompatible SWNT-platform: SWNT immobilization onto glass slides followed our previously published protocol [24] with specific modifications implemented to ensure sterile conditions. Glass slides were sterilized in step two by overnight immersion in a 3-GPTMS solution (98 % ethanol). The subsequent steps were performed under sterile conditions within a biosafety cabinet. To preserve sterility while transitioning the slides to the oven for 150 °C for 3 h (step 3), we designed stainless-steel boxes and autoclaved them before use. For steps 4 and onward, we used the same customized boxes and added water in sterile vials to keep the humidity below the glass slides during the incubation at 37 °C overnight. Solutions utilized in the process were sterilized using 0.2 μm filter vacuum systems, including the avidin 1 mg/ml Avidin in 10 mM NaHCO₃, and the 2 mM aspartic acid in 0.5 M NaHCO₃.

Mycoplasma Assay: Mycoplasma detection employed the MycoAlert Mycoplasma Detection Kit (Lonza, LT07-701). This kit utilizes an enzymatic reaction with the MycoAlert substrate, converting ADP to ATP. Luminescence readings quantified ATP levels with the Modulus Luminometer (Turner Biosystems). The MycoAlert assay control set (LT07-518) served as a positive control, and the experimental procedure followed the manufacturer's protocol.

Endotoxin Assay: The Gel Clot Limulus Amebocyte Lysate (LAL) "Pyrogent" assay (Lonza, Walkersville, MD, USA) is a qualitative method indicating the presence or absence of endotoxins in samples. This assay relies on an enzymatic pro-clotting cascade triggered by endotoxins, resulting in clot formation. The clotting assay, following the manufacturer's procedure, was conducted in reaction tubes (Lonza, N201). The positive control used was the commercial control standard endotoxin (Lonza, LT07-518).

Cell Culture: The MDA-MB-231 cells (ATCC (HTB - 26)), were incubated at 37 $^{\circ}$ C/100 % Air, and cultured in Leibovitz's L-15 medium supplemented with 10 % fetal bovine serum. The adherent cells were subcultured at about 80 % confluency using TrypLE Express solution (Gibco, 12,604,021).

The MDA-MB-231 triple-negative breast cancer cells were chosen for this study because they are adherent cells that can directly interact with the SWNT platforms. Additionally, these cells are renowned for their aggressive phenotype and active functionality in terms of proliferation and morphology, making them ideal for evaluating changes in cell health and functionality among the substrate groups.

Live/Death fluorescence assays: MDA-MB-231 cells were stained with 1 μ M Calcein AM and 2 μ M Ethidium homodimer-1 for 45 min at room temperature in the dark (Invitrogen, Eugene (L3224)). Calcein AM indicated live cells (Ex/Em: 495/518 nm, green), while EthD-1 marked dead cells (Ex/Em: 528/617 nm, red). Multi-channel fluorescent images were captured using a Keyence microscope.

Apoptosis fluorescence assay: FITC annexin V and Propidium iodide (PI) dyes (BD Biosciences, 556,547) marked apoptotic cells. Working solutions (20 μL of 1x Annexin V and 10 μL of 100 μg ml-1 PI per mL of annexin buffer) were added to the cells and incubated for 15 min at room temperature in the dark. FITC annexin V indicated early apoptosis (Ex/Em: 494/518 nm), while PI, binding to DNA, showed late apoptosis (Ex/Em: 535/617 nm). Multi-channel fluorescent images were captured using a Keyence microscope.

Proliferation: MDA-MB-231 cell growth and proliferation on the different substrates were monitored at 8, 24, 48, 72 h by initially seeding a consistent cell density of 9 × 10^4 cell ml⁻¹ in 2 ml per well. At each time point, triplicates per treatment group were detached, centrifuged, and resuspended in media with PI, 10 μ L of 100 μ g ml⁻¹ PI per mL of annexin buffer. After a 5-min incubation with PI, flow cytometry assessed total and dead cell numbers. Results were normalized per substrate area to facilitate accurate comparisons between glass slides and treated six-well plates.

Contact angle: The Rame-Hart instrument was calibrated using the Rame-Hart combo calibration kit. Nano-pure DI water droplets assessed sample hydrophilicity. Each droplet volume was 0.033 ml, with three consecutive droplets introduced before contact angle measurement. Optical images were taken before and after droplet placement, and DROPimage software (standard edition) was used for precise analysis. Before automatic angle identification, manual adjustment of three ROI indicators was performed: (i) a horizontal baseline for the sample surface, (ii) a rectangular area covering the entire droplet, and (iii) two vertical lines outside the selected rectangular area.

Morphology: MDA-MB-231 cell morphology changes on substrates were assessed at 8, 24, and 48 h using elongation ratio and surface area profiles. A consistent seeding density of 8.5 × 10⁴ cells ml⁻¹ in 2 ml per well was maintained among the different substrates by triplicates. To determine cell surface area, actin staining was employed for enhanced contrast. At each time point, cells were fixed with 4 % paraformaldehyde, rinsed, and permeabilized with 0.3 % Triton X-100. ActinGreen 488 (Invitrogen (R37110)) was used for staining, and cells were imaged after 30 min of incubation. Three images in the center of the platform were captured for each triplicate, for the respective substrate. ImageJ was used to quantify the cell length, width, and area for further analysis.

ImageJ analysis: The cell-count plugin quantified cellular length and width dimensions, calibrated with a known scale bar. The line tool manually measured the longest diameter and the longest perpendicular diameter to the elongation axis for each cell. Surface area analysis involved color thresholding and manual optimization of brightness parameters. The magic wand tool outlined each cell, and the surface area was measured.

MATLAB data analysis: Elongation ratio and cell surface distribution profiles were determined using a loop script, which classified and counted the cells within specific ranges.

Statistical analysis: Values represented the mean of three replicates and standard deviation (SD). Two-way ANOVA Tukey's post hoc test using SAS was performed for experimental results. Significance levels: ns p > 0.05, * $p \le 0.05$, ** $p \le 0.01$, *** $p \le 0.001$, **** $p \le 0.0001$.

3. Results and discussion

3.1. Fabrication of biocompatible SWNT platform

In our previously published method to immobilize SWNT on a glass substrate [24], the resulting platform was not sterile. Considering the delicate nature of the platform, high temperature, UV exposure, and organic solvents cannot be used to sterilize it postproduction. To assure the sterility of the *SWNT* at the end of the five-step procedure, various modifications needed to be performed. The second step of the platform production procedure, immersion in 3-glycidyloxypropyltrimethoxysilane (3-GPTMS) solution, results in sterility due to the high ethanol content in the 3-GPTMS (Fig. 1a). To retain sterility throughout the rest of the platform production process, custom stainless-steel boxes, autoclaved between each use, were utilized. These boxes provided many advantages, including the ability to withstand the high temperature and corrosive chemicals used during the platform production process while also ensuring the humidity, through the addition of sterile water, that is required, Fig. S1.

3.2. Sterility of the SWNT platform

The sterility of the modified SWNT platform (SWNT) was evaluated through analysis of microbial, mycoplasma, and endotoxin contamination after 72 h of incubation in media at 37 °C. The SWNT sterility was compared to the two control platforms, a sterile tissue culture treated plate (PLATE) to validate the sterility of the media, and an autoclaved glass slide (GLASS) to validate the sterility of the slide before the immobilization process and to show the impact of the glass base platforms as compared to the tissue culture treated plastic, on any contaminants (Fig. 2). Bacterial, fungal, and yeast contamination can generally be detected through visual indicators, such as an increase in the turbidity or color changes in the media, which utilizes phenol red as an indicator of changes in pH. None of the three platforms had color changes, a cloudy appearance, or the development of turbid films (Fig. 2a). The presence of mycoplasma was assessed using Lonza's MycoAlert assay, which detects enzymatic mycoplasma activity. Only the mycoplasma kit's positive control showed a signal on the luminometer, indicating the absence of mycoplasma contamination in the test conditions (Fig. 2b). Similarly, bacterial endotoxins were tested with the gel-clot LAL assay. No clotting was found for our three test conditions but was observed in the kit's positive control sample, demonstrating that the test was conducted successfully, and the test samples are endotoxinfree (Fig. 2c). The absence of contamination detected by three different assays assures us that the new SWNT platform development process can be used for sterile tissue culture.

3.3. Cytotoxicity of SWNT platforms on MDA-MB-231

While previous in vitro studies have demonstrated the use of SWNT nanoarrays without notable toxicity [11,32], it is necessary to validate the lack of toxicity in our model since any small changes in platform development can alter how the surface interacts with cells. Determination of whether the platform results in harmful effects on cells is especially important for the development of sensors for reactive species to ensure that any detected analytes are a result of treatment conditions and not the cells' interactions with the platform. We performed three viability assays on a triple negative breast cancer cell line, specifically MDA-MB-231, that was cultivated for 72 h on the SWNT, GLASS, and PLATE, two for cell viability, via fluorescent imaging and flow cytometry, and one to detect early stages of apoptosis, via fluorescent staining. The first cell viability assay was Invitrogen's LIVE/DEAD fluorescent assay, which simultaneously stains live cells with calcein to detect enzymatic activity (green) and dead cells with the impermeable Ethidium homodimer-1, which can interact with nucleic acids (red) only after the rupture of the cellular membrane. As shown in the representative fluorescence images in Fig. 3, there is a clear difference between the cells growing on the SWNT for over 72 h, which had very few dead cells (Fig. 3a and b), compared to the dead cell control group, which consisted of cells that were exposed to 70 % methanol after growing on

the SWNT (Fig. 3c and d). The red/green cells in the images were counted by manual enumeration with ImageJ, the cells growing on the SWNT were healthy with a live population average of 99.6 % \pm 0.2. We also analyzed cell viability by detaching cells from their platforms, adding fluorescent dyes, and quantifying the samples with flow cytometry (Fig. 3e) We found variations among the platforms in the percentage of live cells 8 h after seeding, with GLASS having a lower percent of live cells than SWNT, which was lower than PLATE. We suspect that this difference is a result of the initial cellular interactions with the respective platforms. But, starting 24 h after seeding, the live cell population remained comparable across the three platforms, with an average of 85 % live cells, showing that the interaction with SWNT did not contribute to an increase in cell death for at least 72 h.

In addition to cell viability, we also looked for indicators of early and late-stage apoptosis through the use of fluorescent stains. Healthy cells show a lack of staining, early apoptotic cells are stained green by annexin, which binds to the externalized lipid phosphatidyl serine that is exposed during early apoptosis, and late apoptotic cells are stained red with propidium iodide (PI), which is internalized by cells that have a loss of cell membrane integrity [33]. Fluorescence and bright field imaging show that cells grown on *SWNT* for 72 h have a very small number of cells tagged with either phosphatidyl serine or PI, 2.67 % and 1.33 % respectively, as opposed to the control condition incubated with 70 % methanol, which shows 100 % of cells tagged with both phosphatidyl serine and PI. These results demonstrate a lack of early and late-stage apoptosis when cells are grown on the *SWNT* (Fig. 3f and g).

3.4. Cell growth rate on the SWNT platform

The rate of cell growth is an important characteristic for an in vitro platform. If cells on a new sensing platform grow at a significantly different rate than cells grown on the standard platform, it is possible that the sensors on the new platform will not accurately report the phenomena that is seen on the standard platform. Therefore, we studied the rate of triple negative breast cancer (MDA-MB-231) cell growth on SWNT and compared it to cell growth rates on GLASS and PLATE controls. Cell density was quantified on each substrate at 8, 24, and 48 h after seeding. At each time point, cells were imaged, detached from the substrate, centrifuged, resuspended with PI (a cell viability marker), and analyzed with flow cytometry. The cells continued growing on all three substrates for over 48 h (Fig. 4a). PLATE had consistently higher density due to cells' preference for tissue culture-treated polystyrene over glass, while SWNT and GLASS displayed similar cell density for the first 24 h, SWNT showed a significant increase at 48 h, aligning with PLATE levels (Fig. 4b). Fig. 4c shows an increased dead cell density for *PLATE*, which is attributed to the overall increased density. Despite dead cell proportions being similar for the SWNT and GLASS over time, the number of live cells was greater for SWNT, implying a potentially higher viability. Overall, SWNT does not adversely affect cell viability compared to *GLASS*, but cell growth is reduced when compared to PLATE.

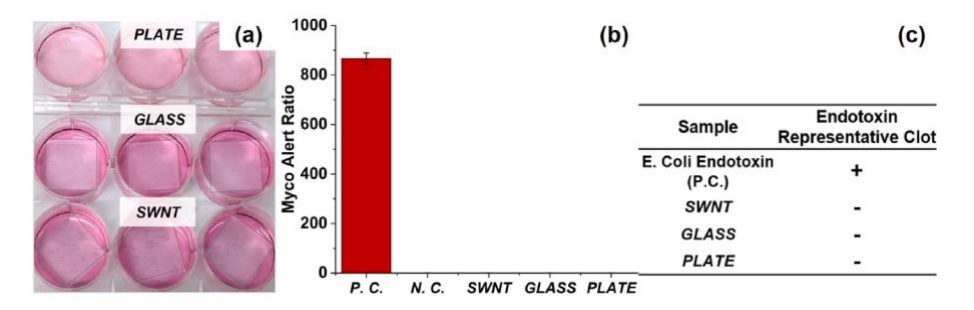


Fig. 2. Sterility assessment of the SWNT after the modification in the multi-step immobilization process (a) Microbial contamination. (b) Mycoplasma, and (c) Endotoxin presence assays.

P·C.: Positive control; N·C.: Negative Control.

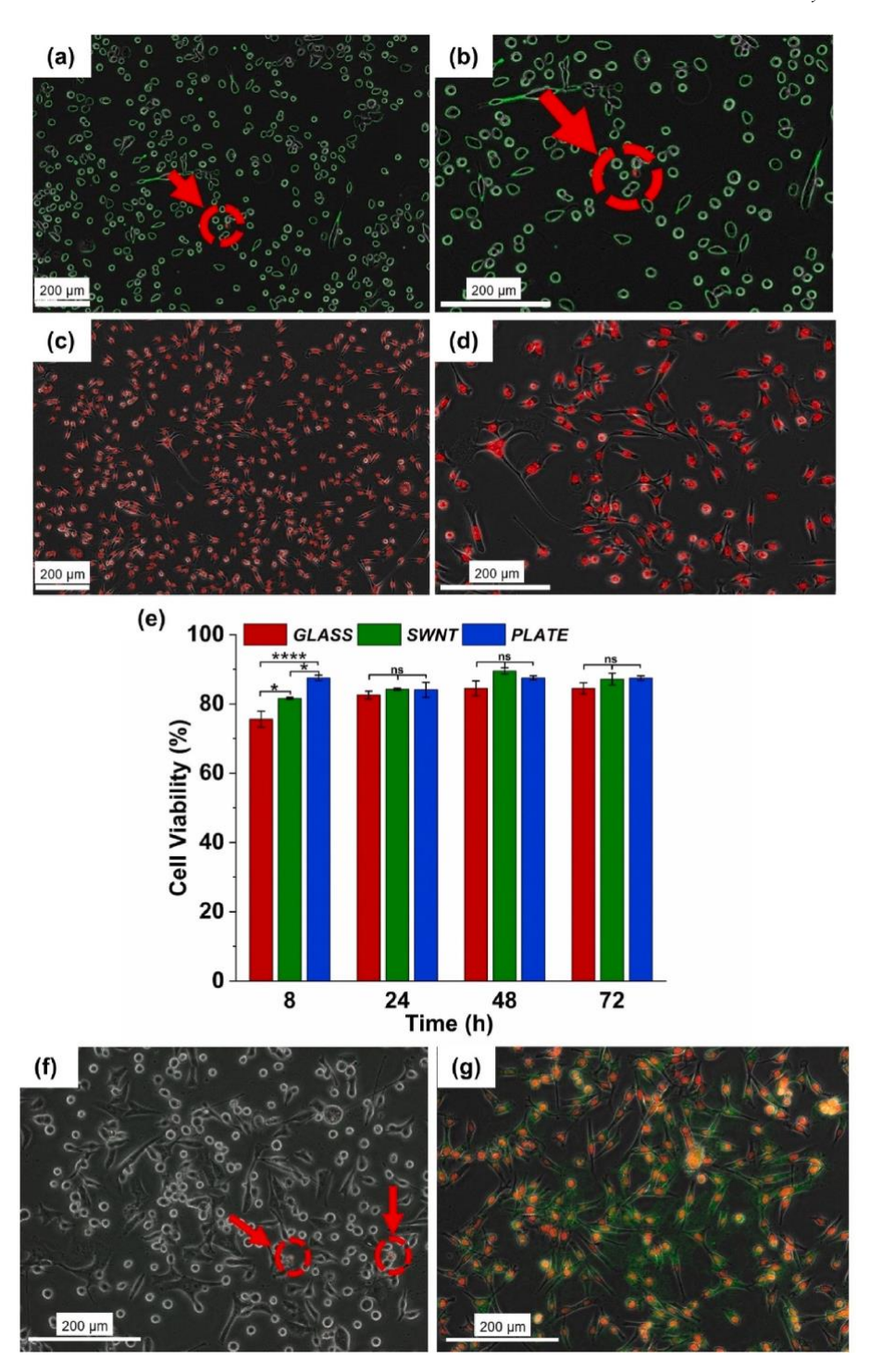


Fig. 3. Viability assay of MDA-MB-231 (triple negative breast cancer) cells growing on the *SWNT* for 72 h. (a–d) Simultaneous live/dead cellular staining images, with live cells stained green (calcein) and dead cells stained red (ethidium homodimer-1). (a) Representative image of healthy cells growing on the *SWNT*, with arrows indicating a few dead cells. (b) Magnified view of (a). (c) Control cells treated with 70 % methanol for cell death induction. (d) Magnified view of (c). (e) Quantification of the live population over time using flow cytometry. Each experiment was performed in triplicate (n = 3) for the respective substrates, values represent the mean \pm standard deviation, with p values calculated by two-way ANOVA Tukey's post hoc test (ns p > 0.05, * $p \le 0.05$, **** $p \le 0.0001$). (f–g) Early/ late apoptosis staining images, early apoptotic cells were stained green (annexin), and late apoptotic cells were stained red (PI). (f) Cells growing on the *SWNT*, arrows show only few cells presenting PI stain. (g) Apoptotic control cells treated with 70 % methanol. n = 3 for both healthy and apoptotic samples. Scale bar $x = 200 \mu m$.

Cell growth, involving initial attachment and subsequent proliferation or growth phase (Fig. 4d), was assessed with an identical seeding density of 180 cells mm⁻² for all substrates. During the attachment phase at 8 h, *PLATE* had the highest attachment (56 %), resulting in 100 cells mm⁻². Glass substrates had a lower initial attachment, with 22 %

on SWNT (40 cells mm⁻²) and 17 % on GLASS (30 cells mm⁻²). These observations emphasize the surface properties' impact on initial cell attachment. In the growth phase, the cell population for all the substrates doubled from 24 to 48 h, consistent with the literature's reported doubling time of approximately 37 h [34]. The proliferation rate was

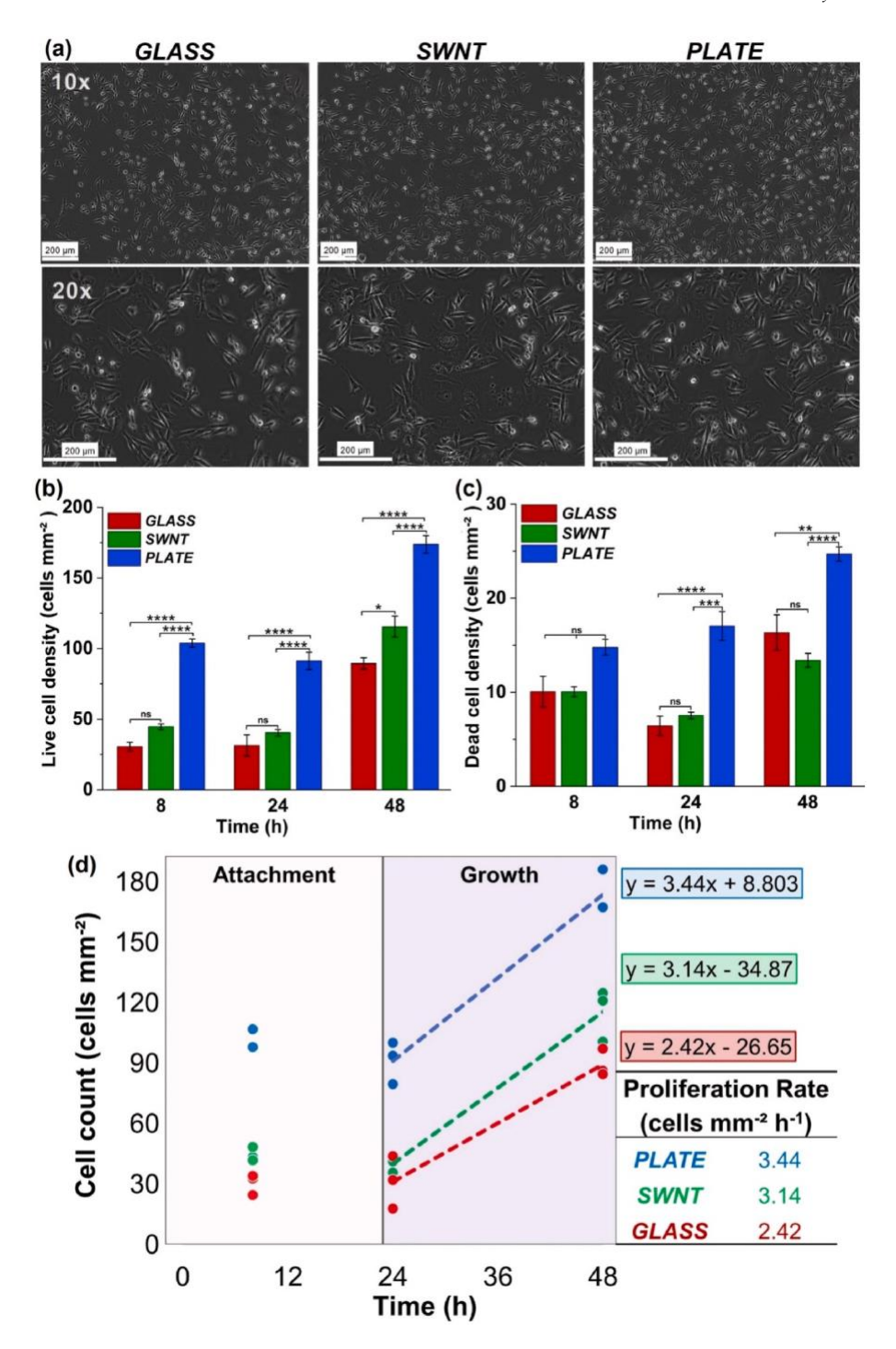


Fig. 4. Cell growth on SWNT. (a) Representative images of MDA-MB-231 breast cancer cell line cultured on various substrates for 48 h, (n = 9) for each substrate at each time point). Scale bar: 200 μ m. (b-c) Quantification of the live (b) and dead (c) cell densities over time for the different substrate groups using flow cytometry. Dead cells were identified with PI. For each time point, the experiment was performed in triplicate (n = 3) for the respective substrates (n = 3). Values represent the mean \pm standard deviation. p values were performed by two-way ANOVA Tukey's post hoc test (ns p > 0.05, * $p \le 0.01$, **** $p \le 0.001$, **** $p \le 0.0001$). (d) Proliferation rate of MDA-MB-231 cells on each substrate, quantified during the growth phase related to the doubling time from 24 to 48 h.

determined by measuring the change in cell density over time during the growth phase. Proliferation rates revealed *PLATE* 's highest (3.44 cells mm⁻² h⁻¹), followed by *SWNT* (3.14 cells mm⁻² h⁻¹) surpassing *GLASS* (2.42 cells mm⁻² h⁻¹). *SWNT*'s chemical surface modification favored proliferation, resembling *PLATE* more than *GLASS*.

Surface properties influence cell attachment and growth, with hydrophilicity being a crucial parameter. Contact angle measurements were tested to validate the hypothesis of varying hydrophilicity levels among the platforms. The contact angles for the *PLATE*, *SWNT*, and *GLASS* were 74.7 \pm 1.4°, 43.3 \pm 1.4°, and 18.3 \pm 0.7° respectively, where smaller angles represent higher hydrophilicity, Fig. S2. *SWNT*'s hydrophilicity lies between the levels for *PLATE* and *GLASS*, aligning with the observed cell attachment trend in Fig. 4. Additionally, surface coating or chemical groups on the surface cause pre-adsorption of media constituents and adhesive proteins, promoting cellular attachment and growth [35]. *PLATE*'s plasma treatment introduces functional groups

[36]. While *SWNT's* favorable surface properties result from the multilayer chemical deposition of amine, avidin, and biotinylated SWNT [37, 38]. Previous studies have demonstrated that amine-modified surfaces lead to preferential cellular attachment due to the pre-adsorption of bovine serum albumin, supporting the observation that *SWNT* has higher cellular attachment than *GLASS* [35].

3.5. Morphology

Cell morphology is a visible representation of a cell's affinity for the substrate and cell's health [39]. If the new sensing platform causes cells to exhibit altered morphologies compared to those exhibited when grown on the standard *PLATE*, it could correlate to altered cell function. Since the goal of the *SWNT* is to detect analytes released from cells, not to alter cell function, it is important to examine the impact of the *SWNT* on cell morphology. To evaluate the effect of the *SWNT* on cell morphology, the cell surface area and elongation ratio were determined on cell images taken at 8, 24, and 48 h post seeding. The elongation ratio (**Equation 1**) provides a method to compare cell length, defined as the longest cell diameter, and cell width, defined as the longest diameter of the cell perpendicular to the length measurement. A ratio close to 1 indicates that the cells are rounded, with similar length and width

dimensions, and higher ratios indicate that cells are spread out and have non-uniform leading edges. Images were analyzed with Image J to quantify the length (L) and width (W) of each cell.

$$r = \frac{L}{W}$$

Equation 1: Elongation ratio as a relationship of length (L), over width (W), the longest perpendicular diameters.

The elongation distribution profiles for the three types of platforms were determined by calculating the percent of cells within specific elongation ratio intervals, 1–1.99, 2–2.99, and so on until 17–17.99 (Fig. 5). At 8 h, the *GLASS* and *SWNT* conditions had a higher percentage of rounded cells represented by an elongation ratio of 1–1.99 (72 % and 60 % respectively) compared to the *PLATE* (40 %). For the elongation ratios of 2 and higher, the percentage of cells for the *PLATE* was highest, followed by the *SWNT*, and lowest for the *GLASS*. These results show that the cells' initial response to *SWNT* is between their response to the *GLASS* and the *PLATE*, cells do not adhere and spread as rapidly on the *SWNT* as they do on their preferred surface (*PLATE*), but they do adhere and spread faster on the *SWNT* than on the *GLASS*. Although the initial cell spreading on the *GLASS* was slower compared to the other platforms, at 24 h the elongation profiles of *SWNT*, *GLASS*, and *PLATE* were

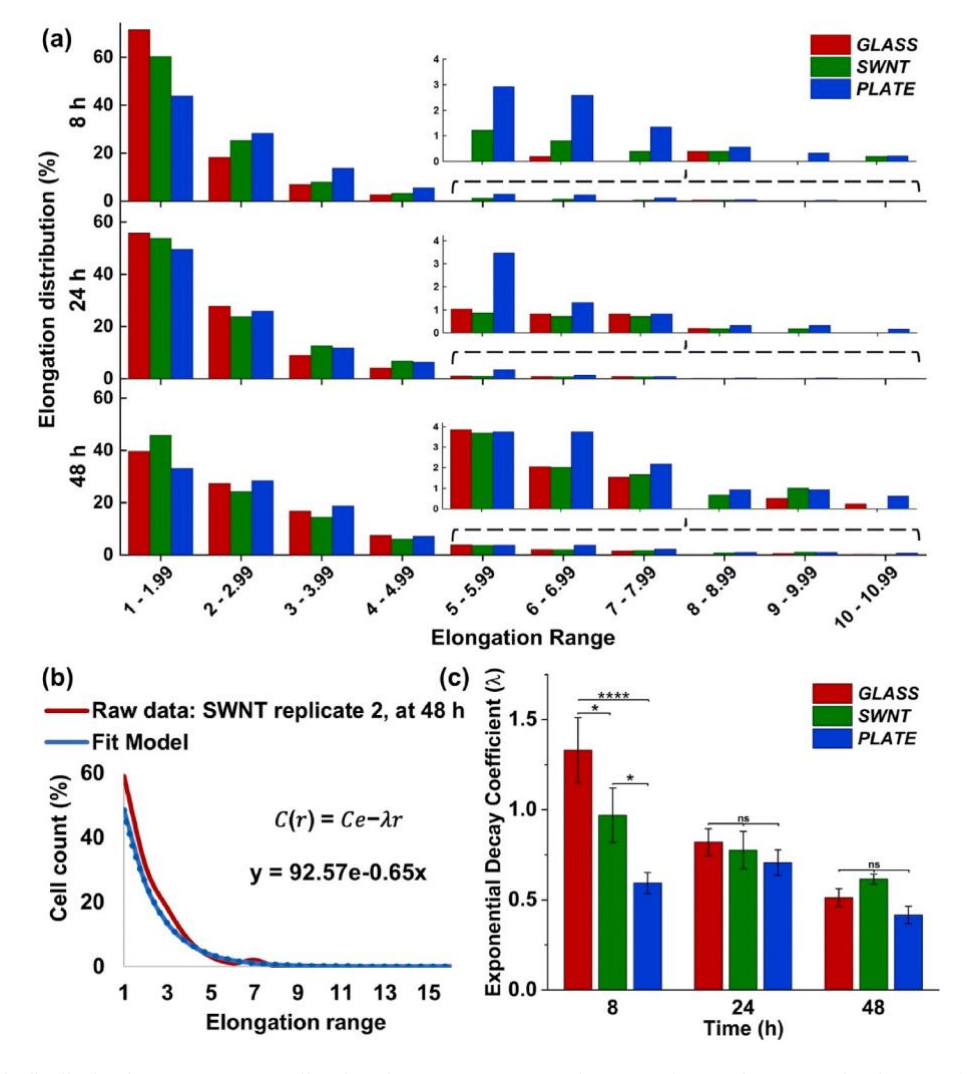


Fig. 5. (a) Elongation ratio distribution for MDA-MB-231 cells cultured on *SWNT*, *GLASS*, and *PLATE* substrates for 8, 24, and 48 h. For each time point, a different set of substrates was used (n = 9). The elongation ratios were sorted in ascending order and grouped into the respective elongation range. (b–c) Quantitative analysis of the elongation distribution using the exponential decay model for the different substrates over time. (b)Exponential decay model (blue) compared to the data (red). (c) Comparison of the exponential decay parameter average (λ) for the substrates over time (n = 3). All the values represent the mean \pm standard deviation, p values were performed by two-way ANOVA Tukey's post hoc test (ns p > 0.05, * $p \le 0.05$, *** $p \le 0.0001$).

comparable. By 48 h, a shift in the distribution of cell elongation was observed for all three platforms, with a decrease in the percent of

rounded cells and an increase in the distribution of elongated ratios. Changes in the elongation ratio profiles are visually evident on the graphs, but in an attempt to quantify these changes, an exponential decay model was used to fit the data (**Equation 2**). While this model typically describes the decay rate over time "N(t)", in our morphological

analysis, it characterizes the rate of decrease in the percent of cells with the increase in elongation ratio "C(r)". Thus, the exponential decay parameter (λ) serves as an indicator of the elongation distribution for the different platforms. A higher I indicates a faster rate of decay, a sharper decline from rounded (ratio = 1) to elongated profiles (ratio ≥ 2), while a smaller (λ) represents a more uniform distribution of cell morphologies. **Equation 2** represents the extended form of the exponential decay equation utilized to fit the model. To determine the position parameter (A) and scale parameter (B) needed for the model, we performed a Generalized Reduced Gradient (GRG) nonlinear method, which aims to find the best-fit parameters to minimize the difference between the model and the actual data points. The model was able to fit the data collected for each of the three platforms at each of the different time points (Fig. 5b-S3).

$$N(t) = N e^{-\lambda t} = C(r) = C e^{-\lambda t}$$

Where:
$$C = {}^{1} * e^{\frac{A}{B}}$$
 and $\lambda = {}^{1}$

$${}^{0} * \frac{A}{B}$$

$$C(r) = {}^{1} * \frac{A}{B} e^{\frac{A}{B} r}$$

Equation 2: Adaptation of the exponential decay model to the morphological application. N(t) is the decrease in quantity N_0 at a constant decay average rate λ over time. Translated into the morphological model C(r) is the decrease in cell count (C_0) at a constant decay average rate (λ) over the elongation ratio range (r).

Comparing λ from the exponential decay equation for each of the platforms (Fig. 5c.) shows that λ_{PLATE} was smaller than λ_{SWNT} , and λ_{SWNT} was smaller than λ_{GLASS} , ($\lambda_{GLASS} > \lambda_{SWNT} > \lambda_{PLATE}$) at the 8 h time point, which represents a sharper decline from rounded (ratio = 1) to elongated profiles (ratio \geq 2) for *GLASS* compared to *SWNT* and PLATE. This information shows that at the 8 h time point the *PLATE* condition has a much more even distribution of elongated and rounded cells, compared to the glass-based platforms which have a higher percentage of rounded cells. Although the initial cell attachment and spreading on the *SWNT* is similar to those on the *GLASS*, cells on the *SWNT* still demonstrated a

higher percentage of elongated cells compared to the GLASS. By the 24 h

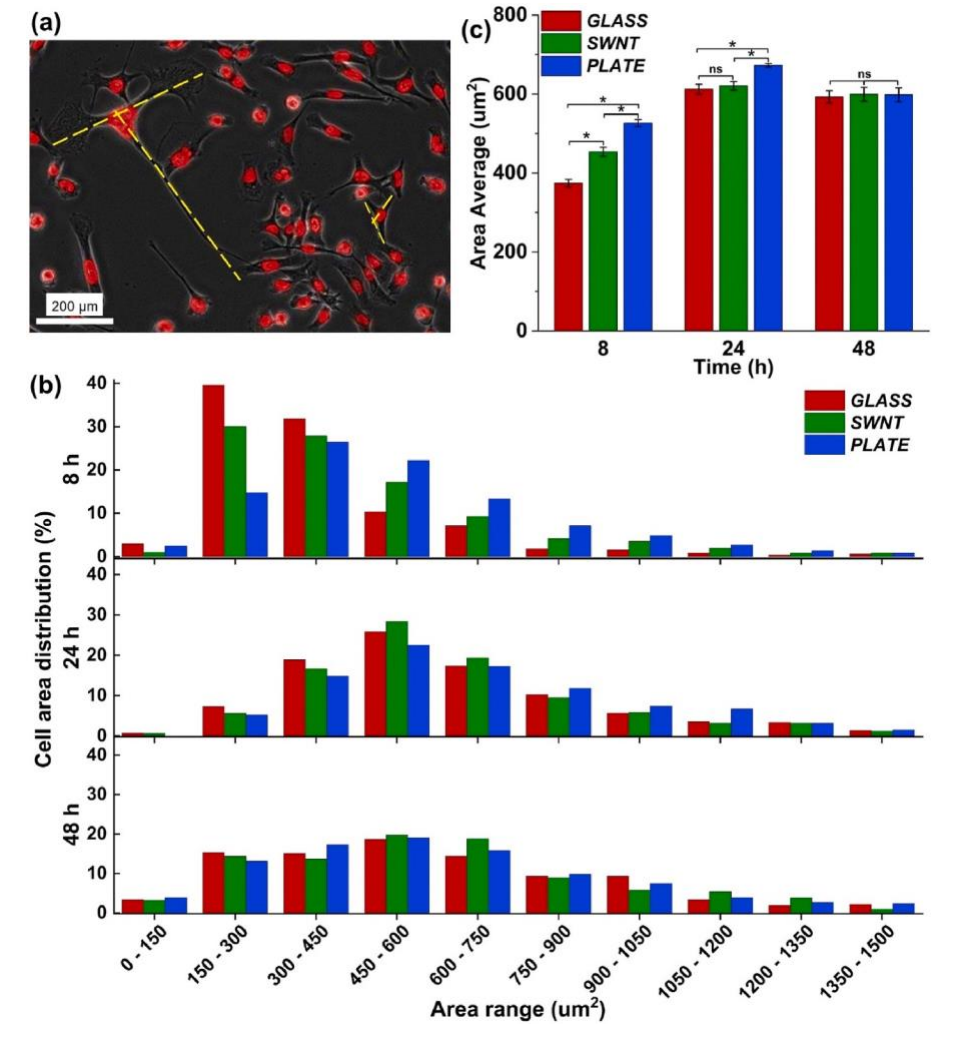


Fig. 6. Morphology analysis based on surface area. (a) Representative image showing the perpendicular extensions of MDA-MB-231 (triple negative breast cancer) cells. (b) Surface area distribution for MDA-MB-231 cells cultured on SWNT compared with that on GLASS and PLATE for 8 h, 24 h, and 48 h (n = 9). The cells' surface area

Was construct interessenting order and grouped into the respective area range. (c) Average cell area over time for each substrate Analyzioù thos the interessent side mean \pm standard deviation, p values were performed by two-way ANOVA Tukey's post hoc test (ns $p > 0.05$).

and 48 h time points, cells have successfully attached to the surface, and the morphological data represents the interaction of the cells with the surface, eliminating the influence of variations from the initial cell attachment. At these timepoints, the cells on all three platforms have similar elongation profiles, with the λ_{SWNT} , λ_{GLASS} , and λ_{PLATE} showing no statistical differences, indicating that SWNT does not alter cell morphology compared to the control platforms. These findings are consistent with the observed results in the elongation distribution profiles presented in Fig. 5 a, SWNT does not alter cell morphology compared to the control platforms.

While elongation ratio analysis is commonly used, the MDA-MB-231's unique shape led to some instances where elongation ratios suggested a circular morphology in elongated cells with perpendicular extensions from the cell body (Fig. 6a). Therefore, we sought to further validate the data by quantifying the surface area of the cells. Cell surface area distribution profiles were determined by classifying the percentage of cells within defined area ranges (Fig. 6b). A comparison of the average surface area of cells for each time point was determined to allow for statistical analysis of differences between the cell surface area on the three platforms (Fig. 6c).

Rounded cells display a smaller surface area compared to elongated cells, therefore it is not surprising that at the 8 h time point the *PLATE* condition, which had higher elongation ratios compared to the other two platforms, had significantly higher cell surface areas. The surface area analysis shows that the *SWNT* had significantly higher values than *GLASS*, bringing the *SWNT* condition closer to that seen for the *PLATE*, the same as what is seen in the elongation ratios (Fig. 6b and c). Cell spreading is noticeable at 24 h among all the substrates, with fewer rounded cells in the 0–300 μ m² range, and a greater cell percentage in higher surface areas. After the cell doubling time, a new population of rounded cells is represented at 48 h, leading to a more uniform size distribution with no significant difference among the substrates (Fig. 6b and c).

The trends in attachment and elongation seen among the substrates align with the proliferation rates in Fig. 4, which is consistent with the literature describing cell adhesion as the foundation for cell proliferation [39] Multiple factors contribute to improved cell spreading and adhesion on *SWNT* compared to *GLASS*, the topographic structure of carbon nanotubes has demonstrated enhanced cell interactions in diverse scaffolds [40,41]. This feature is primarily attributed to the pronounced aspect ratio of *SWNT* [42,43], and to the graphene surface inner cavities that mimic the extracellular matrix porosity and favor the adsorption of cell-secreted adhesive proteins and other biomolecules [42,44]. These findings suggest that the *SWNT* promotes cell spreading through a combination of chemical and physical factors including structural properties.

4. Conclusion

In summary, we re-designed the multi-step process for immobilizing carbon nanotubes to a glass substrate to create a sterile platform that can be used in vitro. We also performed an in-depth investigation on the impact of the SWNT on cells. The newly developed protocol results in a sterile SWNT platform that does not show any significant cytotoxic events for at least 72 h. The proliferation and morphology profiles of cells growing on the SWNT were comparable to that of cells growing on tissue culture-treated plates, despite the lower initial cell attachment rate of the cells on SWNT. Overall, our study provides compelling evidence that the glass-based carbon nanotube platform favors cell health and function. The even nanotube distribution of this biocompatible sensorial platform represents a crucial step toward expanding our spatial and temporal understanding of extracellular analytes in cellular communication [11].

CRediT authorship contribution statement

Ivon Acosta-Ramirez: Writing – review & editing, Writing – original draft, Visualization, Validation, Supervision, Software, Methodology, Investigation, Formal analysis, Data curation, Conceptualization. Carley Conover: Software, Methodology, Investigation, Data curation. Jacob Larsen: Software, Data curation. Portia N.A. Plange: Investigation. Ufuk Kilic: Writing – original draft, Investigation. Becca Muller: Investigation. Nicole M. Iverson: Writing – review & editing, Visuali- zation, Validation, Supervision, Resources, Project administration, Funding acquisition, Conceptualization.

Declaration of competing interest

The authors declare the following financial interests/personal relationships which may be considered as potential competing interests:

Nicole M Iverson reports financial support was provided by National Institute of Health. Nicole M Iverson reports financial support was provided by National Science Foundation. If there are other authors, they declare that they have no known competing financial interests or personal relationships that could have appeared to influence the work reported in this paper.

Data availability

Data will be made available on request.

Acknowledgements

We acknowledge National Institute of Health [grant number 5R35GM138245-02], National Science Foundation [grant number NSF OIA-2044049], the University of Nebraska-Lincoln Office of Undergraduate Research & Fellowships (URF) and Undergraduate Creative Activities and Research Experiences (UCARE) program, funded in part by gifts from the Pepsi Quasi-Endowment and Union Bank and Trust. We would also like to thank Dirk Anderson from the UNL Center for Biotechnology Flow Cytometry Core Facility and Iverson lab members for supporting this study.

Appendix A. Supplementary data

Supplementary data to this article can be found online at https://doi.org/10.1016/j.ab.2024.115582.

References

- M. Kandouz, Intercellular communication in cancer, Intercell. Commun. Cancer (2015) 1–366.
- [2] V.O. Shender, G.P. Arapidi, M.S. Pavlyukov, P.V. Shnaider, K.S. Anufrieva, G. A. Stepanov, V.M. Govorun, The role of intercellular communication in cancer progression, Russ. J. Bioorg. Chem. 44 (2018) 473–480.
- [3] P.W. Barone, S. Baik, D.A. Heller, M.S. Strano, Near-infrared optical sensors based on single-walled carbon nanotubes, Nat. Mater. 4 (2005) 86–92.
- [4] D. Roxbury, P.V. Jena, R.M. Williams, B. Enyedi, P. Niethammer, S. Marcet, M. Verhaegen, S. Blais-Ouellette, D.A. Heller, Hyperspectral microscopy of near-infrared fluorescence enables 17-chirality carbon nanotube imaging, Sci. Rep. 5 (2015) 1-6.
- [5] M.S. Strano, A.A. Boghossian, W.-J. Kim, P.W. Barone, E.S. Jeng, D.A. Heller, N. Nair, H. Jin, R. Sharma, C.Y. Lee, The chemistry of single-walled nanotubes, MRS Bull. 34 (2009) 950–961.
- [6] A.J. Gillen, A.A. Boghossian, Non-covalent methods of engineering optical sensors based on single-walled carbon nanotubes, Front. Chem. 7 (2019) 1–13.
- [7] J. Pan, F. Li, J.H. Choi, Single-walled carbon nanotubes as optical probes for biosensing and imaging, J. Mater. Chem. B 5 (2017) 6511–6522.
- [8] D.P. Salem, X. Gong, A.T. Liu, K. Akombi, M.S. Strano, Immobilization and function of nir-fluorescent carbon nanotube sensors on paper substrates for fluidic manipulation, Anal. Chem. 92 (2020) 916–923.
- [9] D.A. Heller, H. Jin, B.M. Martinez, D. Patel, B.M. Miller, T.K. Yeung, P.V. Jena, C. Ho bartner, T. Ha, S.K. Silverman, M.S. Strano, Multimodal optical sensing and analyte specificity using single-walled carbon nanotubes, Nat. Nanotechnol. 4 (2009) 114–120.

- [10] J.Q. Zhang, A.A. Boghossian, P.W. Barone, A. Rwei, J.H. Kim, D.H. Lin, D.A. Heller, A.J. Hilmer, N. Nair, N.F. Reuel, M.S. Strano, Single molecule detection of nitric oxide enabled by d(AT)(15) DNA adsorbed to near infrared fluorescent singlewalled carbon nanotubes, J. Am. Chem. Soc. 133 (2011) 567–581.
- [11] S. Kruss, D.P. Salem, L. Vukovi'e, B. Lima, E. Vander Ende, E.S. Boyden, M.S. Strano, High-resolution imaging of cellular dopamine efflux using a fluorescent nanosensor array, Proc. Natl. Acad. Sci. USA 114 (2017) 1789–1794.
- [12] T.V. Galassi, P.V. Jena, J. Shah, G. Ao, E. Molitor, Y. Bram, A. Frankel, J. Park, J. Jessurun, D.S. Ory, A. Haimovitz-Friedman, D. Roxbury, J. Mittal, M. Zheng, R. E. Schwartz, D.A. Heller, An optical nanoreporter of endolysosomal lipid accumulation reveals enduring effects of diet on hepatic macrophages in vivo, Sci. Transl. Med. 10 (2018) 1–11.
- [13] J. Dong, D.P. Salem, J.H. Sun, M.S. Strano, Analysis of multiplexed nanosensor arrays based on near-infrared fluorescent single-walled carbon nanotubes, ACS Nano 12 (2018) 3769–3779.
- [14] P.W. Barone, R.S. Parker, M.S. Strano, In vivo fluorescence detection of glucose using a single-walled carbon nanotube optical sensor: design, fluorophore properties, advantages, and disadvantages, Anal. Chem. 77 (2005) 7556–7562.
- [15] R. Zhang, Y. Zhang, Q. Zhang, H. Xie, W. Qian, F. Wei, Growth of half-meter long carbon nanotubes based on schulz-flory distribution, ACS Nano 7 (2013) 6156-6161
- [16] S.M. Bachilo, M.S. Strano, C. Kittrell, R.H. Hauge, R.E. Smalley, R.B. Weisman, Structure-assigned optical spectra of single-walled carbon nanotubes, Science 298 (2002) 2361–2366.
- [17] Z.W. Ulissi, F. Sen, X. Gong, S. Sen, N. Iverson, A.A. Boghossian, L.C. Godoy, G. N. Wogan, D. Mukhopadhyay, M.S. Strano, Spatiotemporal intracellular nitric oxide signaling captured using internalized, near-infrared fluorescent carbon nanotube nanosensors, Nano Lett. 14 (2014) 4887–4894.
- [18] S.-R. Ryoo, Y.-K. Kim, M.-H. Kim, D.-H. Min, Behaviors of NIH-3T3 fibroblasts on graphene/carbon nanotubes: proliferation, focal adhesion, and gene transfection studies, ACS Nano 4 (2010) 6587–6598.
- [19] J. Zhang, A.A. Boghossian, P.W. Barone, A. Rwei, J.-H. Kim, D. Lin, D.A. Heller, A. J. Hilmer, N. Nair, N.F. Reuel, M.S. Strano, Single molecule detection of nitric oxide enabled by d(AT)15 DNA adsorbed to near infrared fluorescent single-walled carbon nanotubes, J. Am. Chem. Soc. 133 (2011) 567–581.
- [20] N.M. Iverson, M.S. Strano, G.N. Wogan, In vivo delivery of nitric oxide-sensing, single-walled carbon nanotubes, Curr. Protoc. Chem. Biol. 7 (2015) 93–102.
- [21] E.M. Hofferber, J.A. Stapleton, J. Adams, M. Kuss, B. Duan, N.M. Iverson, Implantable nanotube sensor platform for rapid analyte detection, Macromol. Biosci. 19 (2019) e1800469.
- [22] N.M. Iverson, P.W. Barone, M. Shandell, L.J. Trudel, S. Sen, F. Sen, V. Ivanov, E. Atolia, E. Farias, T.P. McNicholas, N. Reuel, N.M.A. Parry, G.N. Wogan, M. S. Strano, In vivo biosensing via tissue-localizable near-infrared-fluorescent single-walled carbon nanotubes, Nat. Nanotechnol. 8 (2013) 873–880.
- [23] A. Barhoum, O. Sadak, I.A. Ramirez, N. Iverson, Stimuli-bioresponsive hydrogels as new generation materials for implantable, wearable, and disposable biosensors for medical diagnostics: principles, opportunities, and challenges, Adv. Colloid Interface Sci. 317 (2023) 102920.
- [24] J.A. Stapleton, E.M. Hofferber, J. Meier, I.A. Ramirez, N.M. Iverson, Single-walled carbon nanotube sensor platform for the study of extracellular analytes, ACS Appl. Nano Mater. 4 (2021) 33–42.
- [25] S.J. Florczyk, F.M. Kievit, K. Wang, A.E. Erickson, R.G. Ellenbogen, M. Zhang, 3D porous chitosan-alginate scaffolds promote proliferation and enrichment of cancer stem-like cells, J. Mater. Chem. B 4 (2016) 6326–6334.
- [26] N.S. Türker, A.Y. O'zer, B. Kutlu, R. Nohutcu, A. Sungur, H. Bilgili, M. Ekizoglu, M. O'zalp, The effect of gamma radiation sterilization on dental biomaterials, Tissue Eng. Regen. Med. J. 11 (2014) 341–349.

- [27] M. Imaninezhad, J. Schober, D. Griggs, P. Ruminski, I. Kuljanishvili, S.P. Zustiak, Cell attachment and spreading on carbon nanotubes is facilitated by integrin binding. Front. Bioeng. Biotechnol. 6 (2018) 1–12.
- [28] M. Vandrovcova, J. Hanus, M. Drabik, O. Kylian, H. Biederman, V. Lisa, L. Bacakova, Effect of different surface nanoroughness of titanium dioxide films on the growth of human osteoblast-like MG63 cells, J. Biomed. Mater. Res. 100 A (2012) 1016–1032
- [29] Z.B. Jildeh, P.H. Wagner, M.J. Scho"ning, Sterilization of objects, products, and packaging surfaces and their characterization in different fields of industry: the status in 2020, Phys. Status Solidi 218 (2021) 2000732.
- [30] S.N. Bose, R.J. Davies, The photoreactivity of T-A sequences in oligodeoxyribonucleotides and DNA, Nucleic Acids Res. 12 (1984) 7903-7914.
- [31] M. Zheng, A. Jagota, E.D. Semke, B.A. Diner, R.S. McLean, S.R. Lustig, R. E. Richardson, N.G. Tassi, DNA-assisted dispersion and separation of carbon nanotubes, Nat. Mater. 2 (2003) 338–342.
- [32] H.G. Sudibya, J. Ma, X. Dong, S. Ng, L.-J. Li, X.-W. Liu, P. Chen, Interfacing glycosylated carbon-nanotube-network devices with living cells to detect dynamic secretion of biomolecules, Angew. Chem. Int. Ed. 48 (2009) 2723–2726.
- [33] Z. Darzynkiewicz, S. Bruno, G. Del Bino, W. Gorczyca, M.A. Hotz, P. Lassota, F. Traganos, Features of apoptotic cells measured by flow cytometry, Cytometry 13 (1992) 795–808.
- [34] J. Samson, M. Derlipanska, O. Zaheed, K. Dean, Molecular and cellular characterization of two patient-derived ductal carcinoma in situ (DCIS) cell lines, ETCC-006 and ETCC-010, BMC Cancer 21 (2021) 790.
- [35] K. Webb, V. Hlady, P.A. Tresco, Relative importance of surface wettability and charged functional groups on NIH 3T3 fibroblast attachment, spreading, and cytoskeletal organization, J. Biomed. Mater. Res. 41 (1998) 422–430.
- [36] J. L., Max J. Lerman, Shin Muramoto, Greg Gillen, John P. Fisher, The evolution of polystyrene as a cell culture material, Tissue Eng. B Rev. 24 (2018) 359–372.
- [37] T. Sordel, F. Kermarec-Marcel, S. Garnier-Raveaud, N. Glade, F. Sauter-Starace, C. Pudda, M. Borella, M. Plissonnier, F. Chatelain, F. Bruckert, N. Picollet-D'hahan, Influence of glass and polymer coatings on CHO cell morphology and adhesion, Biomaterials 28 (2007) 1572–1584.
- [38] M. Crespin, N. Moreau, B. Masereel, O. Feron, B. Gallez, T. Vander Borght, C. Michiels, S. Lucas, Surface properties and cell adhesion onto allylamine-plasma and amine-plasma coated glass coverslips, J. Mater. Sci. Mater. Med. 22 (2011) 671–682
- [39] A.A. Khalili, M.R. Ahmad, A review of cell adhesion studies for biomedical and biological applications, Int. J. Mol. Sci. 16 (2015) 18149–18184.
- [40] R. Lemos, F.R. Maia, R.L. Reis, J.M. Oliveira, Engineering of extracellular matrixlike biomaterials at nano- and macroscale toward fabrication of hierarchical scaffolds for bone tissue engineering, Adv. Nano Biomed. Res. 2 (2022) 2100116.
- [41] P.M. Mendes, Cellular nanotechnology: making biological interfaces smarter, Chem. Soc. Rev. 42 (2013) 9207–9218.
- [42] T. Szyman´ski, A.A. Mieloch, M. Richter, T. Trzeciak, E. Florek, J.D. Rybka, M. Giersig, Utilization of carbon nanotubes in manufacturing of 3D cartilage and bone scaffolds, Materials 13 (2020) 4039.
- [43] T.R. Fadel, F.A. Sharp, N. Vudattu, R. Ragheb, J. Garyu, D. Kim, E. Hong, N. Li, G. L. Haller, L.D. Pfefferle, S. Justesen, K.C. Herold, T.M. Fahmy, A carbon nanotube—polymer composite for T-cell therapy, Nat. Nanotechnol. 9 (2014) 639–647.
- [44] F.M. Tonelli, A.K. Santos, K.N. Gomes, E. Lorençon, S. Guatimosim, L.O. Ladeira, R. Resende, Carbon nanotube interaction with extracellular matrix proteins producing scaffolds for tissue engineering, Int. J. Nanomed. 7 (2012) 4511–4529.